AAS 14-378

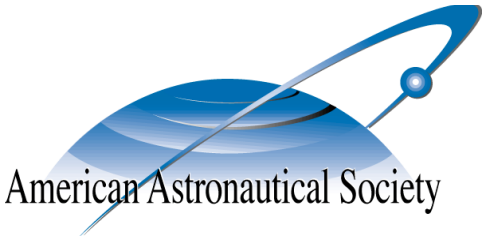

American Institute of
Aeronautics and Astronautics

TOUCHLESS ELECTROSTATIC THREE-DIMENSIONAL DETUMBLING OF LARGE GEO DEBRIS

Trevor Bennett and Hanspeter Schaub

AAS/AIAA Spaceflight Mechanics Meeting

Santa Fe, New Mexico **January 26–30, 2014**

AAS Publications Office, P.O. Box 28130, San Diego, CA 92198

AAS 14-378

TOUCHLESS ELECTROSTATIC THREE-DIMENSIONAL DETUMBLING OF LARGE GEO DEBRIS

Trevor Bennett* **and Hanspeter Schaub†**

Touchless detumbling of space debris is investigated to enable orbital servicing or active debris removal. Using active charge transfer between a tug and debris object, control torques are created to reduce the debris spin rate prior to making any physical contact. In this work, the tug shape is spherical and the debris is assumed to be cylindrical and tumbling. The attitude control goal is to arrest the debris tumbling motion while maintaining a fixed position ahead of the GEO debris object. Prior work has identified the feasibility of electrostatic detumble for one degree of rotational freedom. This work extends the theory to three-dimensional tumbling motion. Using the previously developed Multi-Sphere modeling method for electrostatic forces and torques on non-spherical objects, Lyapunov control theory and numerical simulations are used to demonstrate a stabilizing attitude control.

INTRODUCTION

Non-cooperative electrostatic control sees application in orbital space debris mitigation for bodies in Geosynchronous orbit such as defunct dual-spin spacecraft or spent upper-stage boosters. These objects of interest tumble at rates exceeding the capabilities of current docking or grappling techniques. Orbital servicing is a challenging space mission concept that requires an active host vehicle to approach, and mechanically interface with a defunct satellite or satellite component.[1,2,3] If the debris is tumbling, the process of docking onto the debris presents challenges and collision risks. Advanced docking systems such as those being developed by MDA discuss a maximum tumble rate of 1 degree/second for autonomous docking.[4] A touchless method of detumbling a passive object would greatly simplify the rendezvous and docking phase of an orbital servicer, and is the focus of this paper. Reference 5 discusses how electrostatic torque can be controlled to apply torques on a spinning debris object without requiring physical contact as shown in Figure 1. The charging is controlled through an electron or ion gun that charges the tug positively or negatively and the debris positively. Such electrostatic actuation with a passive object is called an Electrostatic Tractor (ET), and is being considered for both large GEO debris mitigation[6,7,8] as well as touchless asteroid spin control.[9,10]

Electrostatic actuation of spacecraft has been explored since the 1960s. Reference 11 shows that the Geosynchronous Orbit environment is a candidate region where space plasma conditions enable Debye lengths on the order of 100's of meters with electrostatic control requiring only Watt-level power requirements. The feasibility of electrostatic control and actuation in space has been explored by several authors exploring both applications and charging dynamics[12,13,14,15,16,17,18] Electrostatic

*Graduate Research Assistant, Aerospace Engineering Sciences, University of Colorado.
†Professor, Department of Aerospace Engineering Sciences, University of Colorado, 431 UCB, Colorado Center for Astrodynamics Research, Boulder, CO 80309-0431

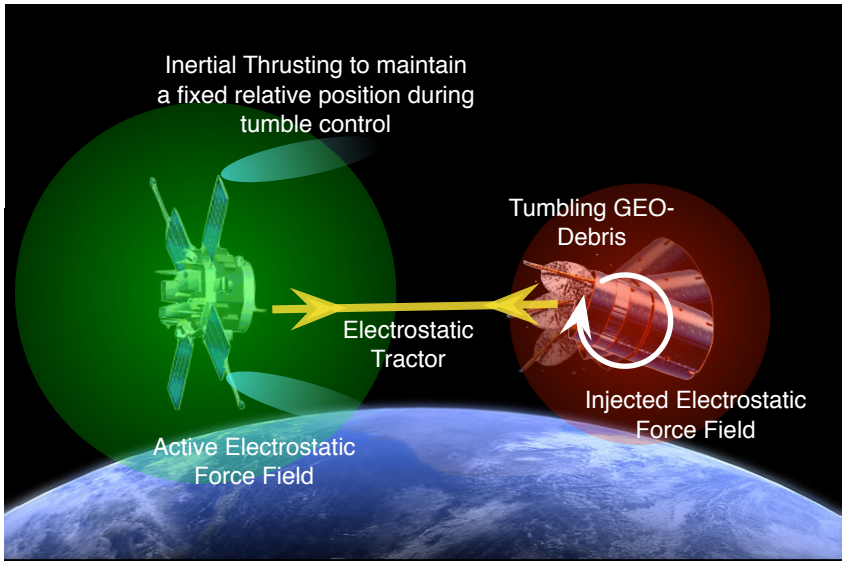

Figure 1. Electrostatic Detumbling Concept Illustration.

detumble control could reduce the non-cooperative spacecraft rates prior to using other proximity or docking operations while minimizing onboard fuel usage.

The prospect of fuel efficiency in implementing electrostatic actuation is counterbalanced by increased complexity and highly-coupled nonlinear differential equations.[19] Electrostatic interaction between two spacecraft in a vacuum is accurately determined using finite element methods; however, these methods are computationally expensive and time intensive. Overcoming the modeling complexity enables onboard and autonomous spacecraft control through control of relative potentials on itself and another spacecraft or uncooperative body. Stevenson and Schaub introduce and validate a new method called the Multi-Sphere Method (MSM)[19,20] that accurately approximates electrostatic interaction between spacecraft with orders of magnitude less computational time enabling attitude simulations and control developments. The multi-sphere method, summarized in the following sections, partitions the spacecraft volume into a series electrostatic conducting spheres constrained by a spacecraft potential. Using the recently developed MSM technique, Reference 5 studies the charged relative one-dimensional rotational dynamics of a non-cooperative cylinder and a spherical charge-controlled spacecraft. A Lyapunov control development is provided to analytically guarantee global stability of the spin rate with the nominal ET force is assumed to be zero. The MSM result is used in numerical simulation to validate the expected control performance for all these 1-D despin scenarios. An experimental setup demonstrating electrostatic detumble control for 1-D cylinder rotation is discussed in Reference 21.

The focus of this study is the generalization of the one-dimensional detumble control to three-dimensional detumble control using Lyapunov control techniques and the MSM electrostatic model. The study will consider a non-cooperative tumbling cylinder and a spherical control spacecraft separated by a fixed distance. Upper stage rocket bodies form a large component of GEO debris, justifying the assumption of a cylindrical debris shape for the scope of this paper. The objects are assumed to be in deep space, and no gravitational attraction is assumed. Reference 5 postulates a simplified electrostatic torque model with separation of the voltage and attitude dependent components. This assumption is shown to be good if the separation distance is at least 3-4 craft radii. In

this paper this separation of voltage and attitude dependency of the electrostatic torque is investigated in more detail for debris undergoing three-dimensional rotations. Of interest is how torque equilibriums impact the convergence of the general tumbling scenario, the stability of such equilibria, and the development of a general detumble ET control algorithm. The following sections detail the Multi-Sphere Method, the torque development, and proposed control structure. The paper concludes with numerical simulations and analysis.

MULTI-SPHERE METHOD

The Multi-Sphere Method (MSM) represents the complete spacecraft electrostatic charging model as a collection of spherical conductors dispersed through the body[19] to provide induced charging effects consistent with finite element methods. The cylinder configuration representative of the above mentioned rocket bodies and defunct spacecraft is represented in Figure 2.

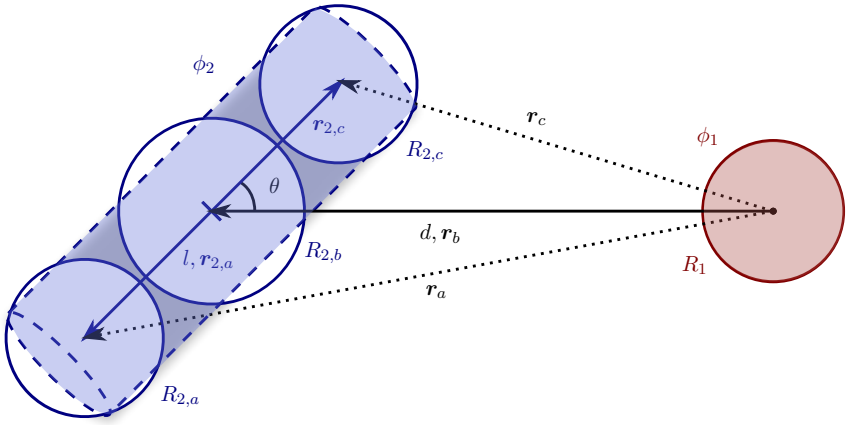

Figure 2. 3 sphere MSM cylinder and spherical spacecraft configuration.

The three sphere MSM approximation provides sufficient force and torque accuracy for the separation distances considered.[20] All three conducting spheres are centered along the long axis of the cylinder which provides a diagonal moment of inertia matrix and symmetric charging. These two simplifications are crucial in the analysis presented here. The MSM geometric parameters used in this analysis are shown in Table 1.

Table 1. MSM parameters for cylinder detumble system.

Parameter	Value	Units	Description
d	15	m	Object center-to-center separation
l	1.1569	m	Outer sphere offset
R_a,R_c	0.5909	m	Outer sphere radius
R_b	0.6512	m	Central sphere radius

The cylinder in this study tumbles with three rotational degrees of freedom. Figure 2 presents a planar view of the setup for clarity. The modeled control parameters are the separation distance d of the mass centers and the controlled potentials ϕ_1 and ϕ_2 corresponding to the commanding

spacecraft and cylinder respectively. The inertial coordinate system fixed to the controlled spherical spacecraft has the y axis pointed along the relative distance vector, the z axis pointed up, and the x axis completing a right-handed system. The cylinder has body fixed coordinates with $\hat{\boldsymbol{b}}_1$ through the long axis with $\hat{\boldsymbol{b}}_2$ and $\hat{\boldsymbol{b}}_3$ in the right handed transverse directions. The cylinder attitude is characterized by a rotation about the inertial z axis θ, and a pitch angle defined as a positive $\hat{\boldsymbol{b}}_2$ rotation. The rotation angle $\theta = 0$ and the pitch angle $\psi = 0$ when the cylinder $\hat{\boldsymbol{b}}_1$ axis is aligned with the vector from the commanding spacecraft mass center to the cylinder mass center.

The electrostatic forces are determined by the charges residing on each sphere. These result from the prescribed electric potentials, according to the self and mutual capacitance relationships in Eq. (1), where $k_c = 8.99 \times 10^9$ N·m^2/C^2 and q_i is the charge of each sphere.[22,23]

$$\phi_i = k_c \frac{q_i}{R_i} + \sum_{j=1, j\neq i}^{m} k_c \frac{q_j}{r_{i,j}} \tag{1}$$

where R_i denotes the radius of the i^{th} conducting sphere and $r_{i,j}$ denotes the vector between the i^{th} and j^{th} conducting spheres. These relations can be represented in matrix form

$$\begin{bmatrix} \phi_1 \\ \phi_2 \\ \vdots \\ \phi_2 \end{bmatrix} = k_c \begin{bmatrix} 1/R_1 & 1/r_a & 1/r_b & 1/r_c \\ 1/r_a & 1/R_{2,a} & 1/l & 1/2l \\ 1/r_b & 1/l & 1/R_{2,b} & 1/l \\ 1/r_c & 1/2l & 1/l & 1/R_{2,c} \end{bmatrix} \begin{bmatrix} q_1 \\ q_a \\ q_b \\ q_c \end{bmatrix} \tag{2}$$

Inverting the matrix multiplying the charge at a given instant in time produces the forces and torques on the cylinder given by the summations

$$\boldsymbol{F}_2 = k_c q_1 \sum_{i=a}^{c} \frac{q_i}{r_i^3} \boldsymbol{r}_i \tag{3}$$

$$\boldsymbol{L}_2 = k_c q_1 \sum_{i=a}^{c} \frac{q_i}{r_i^3} \boldsymbol{r}_{2,i} \times \boldsymbol{r}_i \tag{4}$$

The controlling sphere and cylinder remain at a constant separation distance requiring a thrusting force to counter-balance the net attractive or repulsive electrostatic forces on the commanding spacecraft. The control development assumes the necessary thrust force is present and though the system is moving in space the fixed relative distance assumes that the spacecraft can be considered stationary for the control development and analysis.

ANALYTIC TORQUE DEVELOPMENT

The expression for torque in Eq. (4) provides an analytic torque expression. However, the square matrix has size equivalent to the number of spheres and couples the control potential ϕ and attitude information. The equilibrium states and stability of the system are more easily explored using an analytic approximation of the MSM torque.

One-Dimensional Representation

As shown by Reference 5, if the separation distance is sufficiently large, the potential and attitude influence on the electrostatic torque can be separated as shown in Eq. (5) where θ represents a 1-D attitude measure.

$$L = \gamma f\left(\phi\right) g\left(\theta\right) \tag{5}$$

The separation of the potential dependence function $f(\phi)$ and the orientation dependence function $g(\theta)$ allows for a simplified analytic study in-place of the matrix inversion necessary in Eq. (2). Without loss of generality, the non-cooperative cylinder has the same potential magnitude, that is $\phi_2 = |\phi_1|$, and is assumed to be always positive.[5] Thus, the voltage dependency function is set to:[5]

$$f\left(\phi\right) = \phi|\phi| \tag{6}$$

The orientation angle dependency explored by Reference 5 presents Eq. (7) as the analytic representation. Reference 5 also demonstrates more complicated torque surfaces character at close proximity due to induced charging properties. Implementation at a separation distance of $d = 15\ m$ accurately approximated the torque surface with a correlation of $R^2 = 0.9998$ and the tuned scaling parameter $\gamma = 2.234 \times 10^{-14}$.[5]

$$g(\theta) = \sin(2\theta) \tag{7}$$

Using the potential and orientation dependency functions in Eq. (5) provides a separable form base function to approximate the MSM torque profile. Setting $\theta = 0$ when the slender axis of the cylinder is aligned with the inter-spacecraft vector allows for a 1-D spin rate control function $f(\phi)$ to be developed.

Generalization for Attitude Coordinates

The control form presented in Eq. (5) and accompanying orientation angle dependency in Eq. (7) are generalized for 3-D tumbling motion by Eq. (8) and general attitude coordinates σ.

$$L = \gamma f\left(\phi\right) g\left(\boldsymbol{\sigma}\right) \tag{8}$$

The induced charge effect of the MSM spheres dictates that the $g(\boldsymbol{\sigma})$ function is dependent on separation distance. This study considers a fixed separation distance of $d = 15\ m$ that exceeds major induced charging effect torque contributions. Assuming a fixed separation distance and surface potential, Figure 3 illustrates the resulting electrostatic torques on the cylinder where the attitude is parameterized using a 3-2-1 Euler angle sequence through θ, ψ, and a rotation about $\hat{\boldsymbol{b}}_1$. Because of the axi-symmetric shape of a cylinder and MSM sphere distribution, the torque will not depend on the rotation about the first body axis $\hat{\boldsymbol{b}}_1$. The torque profile estimate using the separable dependency functions and corresponding error to the MSM prediction is shown in Figure 3. The torque function is approximated. Clearly visible in Figure 3 are the equilibrium surfaces present when either yaw or pitch achieves 0° or 90°. The character of Figure 3 is symmetric and suggests a simpler generalization of the cylinder attitude coordinates. As stated earlier, the torque does not have a component about the cylinder $\hat{\boldsymbol{b}}_1$ axis. Therefore the torque axis and projection angle about the torque axis are defined.

$$\hat{\boldsymbol{e}}_L = \hat{\boldsymbol{b}}_1 \times -\hat{\boldsymbol{r}} \tag{9}$$

$$\Phi = \cos^{-1}\left(\hat{\boldsymbol{b}}_1 \cdot (-\hat{\boldsymbol{r}})\right) \tag{10}$$

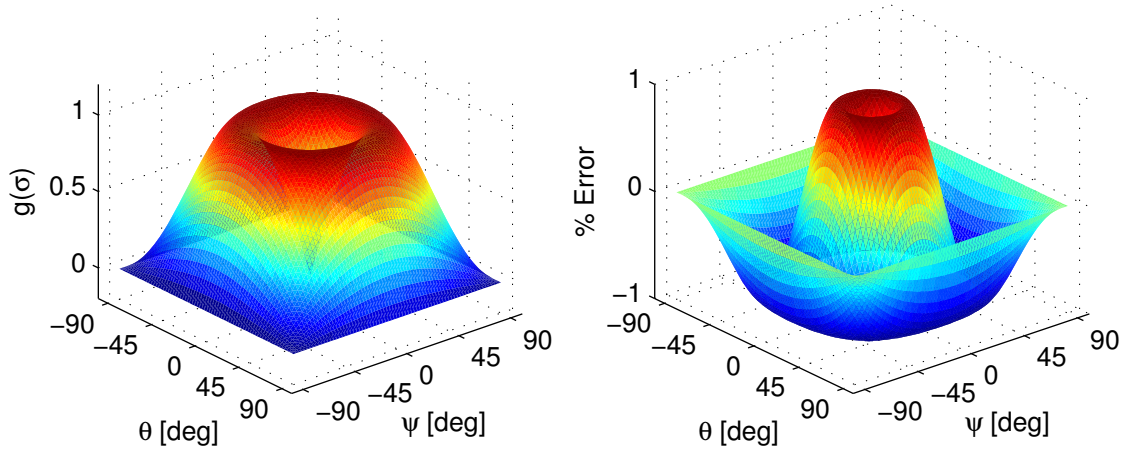

(a) Base function as a function of attitude

(b) Error between base function and MSM

Figure 3. Normalized torque surface and corresponding error at a separation distance of $d = 15\ m$ for $V_1 = -30\ kV$ and $V_2 = 30\ kV$.

where $\hat{\boldsymbol{r}}$ is the unit direction from the commanding spacecraft mass center to the tumbling body mass center. The orientation dependency function assumes the form in Eq. (11).

$$g(\boldsymbol{\sigma}) = \sin(2\Phi) \tag{11}$$

The projection angle orientation dependency form captures the behavior previously studied by Reference 5 for the 1-D case. For example, if the pitch angle were zero, the projection angle would be the rotation angle θ and the control collapses to the 1-D form. Implementation of the projection angle formulation captures the torque surface in Figure 3 with a correlation of $R^2 = 0.9998$ when separated at $d = 15$ m. The MSM predicted torque surface is sensitive to separation distance, and the fit quality provided by Eq. (11) decreases rapidly as the separation distance diminishes. The sensitivity to separation distance is shown in Figure 4 where the MSM predicted torque is shown for a separation distance of $d = 15$m and $d = 2$ m respectively. The change in torque surface character is clearly visible in Figure 4 where the torques for the $d = 15$ m separation and $d = 2.5$ m separation distances are shown respectively. Evident in Figure 4, the torque surface deforms in both profile at a fixed potential and the torque strength between the positive and negative potentials as the separation distance is varied. To capture the variation in character, a more general orientation dependency function is required.

Generalization of Orientation Dependency Function

The quality of the fit degrades as the separation distance decreases due to the induced charging effects predicted by MSM but not by the analytic approximation in Eq. (8). The analytic form is extended to

$$L = f(\phi) \sum_{m=1}^{n} \gamma_m g_m(\boldsymbol{\sigma}) \tag{12}$$

where n is the number of terms in the desired approximation and γ_m is the coefficient of the m^{th} term. The separable form, used to avoid matrix inversion of the MSM model, allows the summation of an infinite number of representative approximation functions to be used in equilibrium and

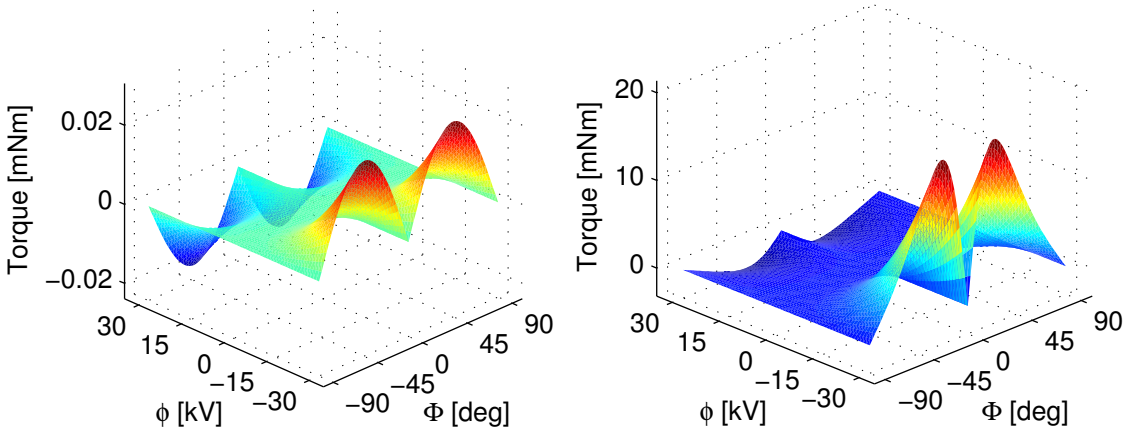

(a) Separation $d = 15$ m

(b) Separation $d = 2.5$ m

Figure 4. MSM torque surfaces at a separation distances of $d = 2.5$ m and $d = 15$ m for $V_1 = -30\ kV$ and $V_2 = 30\ kV$.

Lyapunov analysis. Inclusion of additional terms in the analytic approximation enables more accurate close proximity fits to the MSM torque representation. Greater quality in the approximation fit provides more confidence in the stability analysis. Referring to Figure 3, the error plot can be approximated by a scaled $\sin(4\Phi)$. This suggests a Taylor series like approximation in Eq. (13).

$$\sum_{m=1}^{n} \gamma_m g_m(\boldsymbol{\sigma}) = \sum_{m=1}^{n} \gamma_m \sin(2m\Phi) \tag{13}$$

The γ_m terms are addressed in part by the following analysis. Applying the general expansion form to the close proximity profiles in Figure 4 yields the improved approximation shown in Figure 5. The profiles shown in Figure 5 are normalized about the max value. This removes the search for scaling terms and more clearly exhibits fit quality improvement. Additional terms are included separately for both the attractive torque case shown on the left, where $f(\phi) < 0$, and the repulsive case shown on the right, where $f(\phi) > 0$. The two term approximation is explicitly:

$$g(\boldsymbol{\sigma}) = \sum_{m=1}^{2} \frac{m!}{d^{2(m-1)}} \sin 2m\Phi \tag{14}$$

The separation distance appears in the denominator as a "stiffness" like term. Therefore, as the separation distance grows, the higher order terms tend towards zero. This stiffness formulation increases the fit quality across the entire separation distance regime. While beneficial to have the general form, only the first order term is necessary in the following analysis because the separation distance is held fixed at $d = 15$ m. A separation distance of $d = 15$ m is considered beyond close proximity and therefore falls within a more likely operation range.

CONSTANT POTENTIAL EQUILIBRIUM STATES

The following developments require that the function $f(\phi)$ in Eq. (12) be invertible and posses the property $f(\phi)\phi \geq 0$ enforced by Eq. (6) criteria.[5] The three-dimensional rotational equations

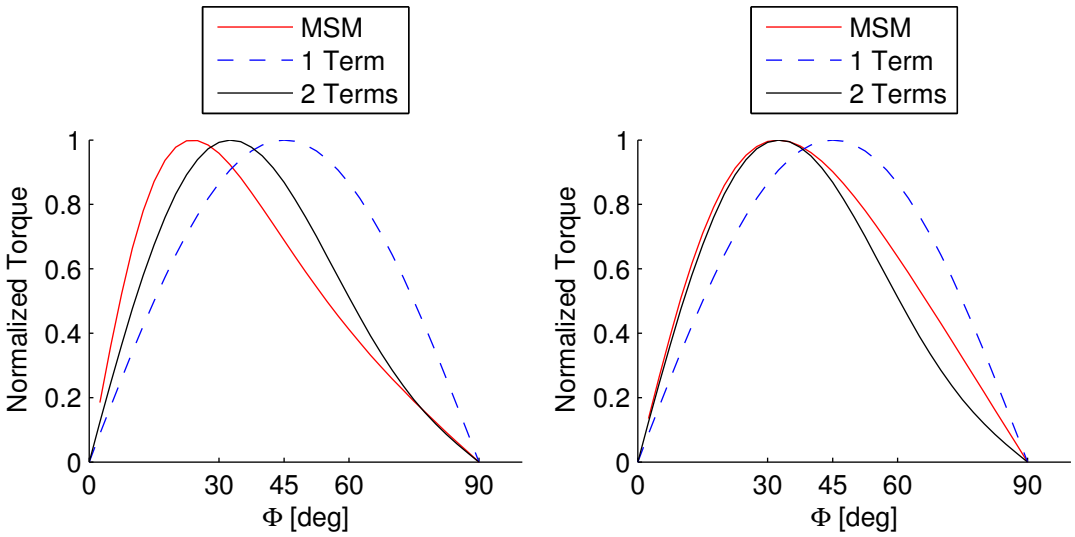

(a) Attractive, $d = 2.5$ m, $f(\phi) < 0$ (b) Repulsive, $d = 2.5$ m, $f(\phi) > 0$

Figure 5. Additional terms in $g(\sigma)$ approximation of MSM.

of motion are given by

$$I\dot{\boldsymbol{\omega}} + \boldsymbol{\omega} \times I\boldsymbol{\omega} = \boldsymbol{L} \tag{15}$$

The equations of motion are re-cast by defining a projection angle principal coordinate system with principal moments of inertia $I = \text{diag}[I_a \; I_t \; I_t]$.

$$E = \{\hat{\boldsymbol{b}}_1, \hat{\boldsymbol{e}}_L \times \hat{\boldsymbol{b}}_1, \hat{\boldsymbol{e}}_L\}$$

Noting that the moment of inertia about the torque axis is always perpendicular to $\hat{\boldsymbol{b}}_1$, the simplified generalized equations of motion assume the form in Eq. (16). Reduction of the three dimensional rotational equations of motion to two scalar equations enables the control to only influence torques around the cylinder's transverse $\hat{\boldsymbol{e}}_L$ axis exclusively. Consistent with the assumption of an axi-symmetric geometry, there exists no control authority in the $\hat{\boldsymbol{b}}_1$ axis scalar equation because no cross coupling is present.

$$I_a\dot{\omega}_1 = 0 \tag{16a}$$

$$I_t\dot{\eta} - I_a\omega_1\dot{\Phi}\sin\Phi = 0 \tag{16b}$$

$$I_t\left(\ddot{\Phi}\sin\Phi - \eta^2\frac{\cos\Phi}{\sin^2\Phi}\right) + I_a\omega_1\eta = L \tag{16c}$$

where I_a is the axial moment of inertia, I_t is the transverse moment of inertia, and

$$\eta \equiv -\omega_2(\hat{\boldsymbol{r}}\cdot\hat{\boldsymbol{b}}_2) - \omega_3(\hat{\boldsymbol{r}}\cdot\hat{\boldsymbol{b}}_3) \tag{17a}$$

$$\dot{\Phi}\sin\Phi = -\omega_2(\hat{\boldsymbol{r}}\cdot\hat{\boldsymbol{b}}_3) + \omega_3(\hat{\boldsymbol{r}}\cdot\hat{\boldsymbol{b}}_2) \tag{17b}$$

$$\boldsymbol{L} = -L\hat{\boldsymbol{e}}_L = -f(\phi)\sin(2\Phi)\,\hat{\boldsymbol{e}}_L \tag{17c}$$

The equilibrium conditions occur at points where the torque is zero which requires the sum of the orientation dependency functions equating to zero. The system equilibrium states are present at

projection angle orientations $\Phi = 2\pi n$ for $n = 0, 1, 2, 3$ given the form considered in Eq. (13). Evident in the second scalar equation of motion, Eq. (16b), requires either ω_1, $\dot{\Phi}$, or $\sin(\Phi)$ to be zero for $\dot{\eta}$ to be zero. Study of the torque free Eq. (16c) provides insight into the equilibrium conditions defined by torque free configurations and the conditions from Eq. (16b). Consider the 2 following orientation cases:

Case 1: First assume $\Phi = 0$, that is the cylinder $\hat{\boldsymbol{b}}_1$ axis is aligned with the negative inter-spacecraft separation vector $-\hat{\boldsymbol{r}}$. Multiplying the torque free Eq. (16c) by $\sin^2\Phi$ and inserting $\Phi = 0$ yields the following condition:

$$I_t\eta^2 = 0 \rightarrow \eta = 0 \tag{18}$$

Given this condition, the only way to remain at this point is for $\dot{\eta} = 0$ and therefore $\dot{\Phi} = 0$. This configuration holds if both the projection angle, angle rate, and the perpendicular angle rate η all equal zero. This configuration does not require that the spin about the $\hat{\boldsymbol{b}}_1$ axis go to zero. The third equation of motion clearly highlights the $\sin\Phi = 0$ singularity in the dynamics definitions. The singularity results from the torque axis, described by Eq. (9), being undefined at this orientation. The singular term, for linearized deviations in η behaves as $0/0$ and the departure behavior is unclear. However, given the definition of the projection angle and the torque axis, any angular rate perturbation away from the $\Phi = 0$ equilibria enforces that the perturbation is about the torque axis and therefore no η perturbation is possible and $\eta = 0$ is maintained. Inserting a small perturbation in the projection angle and $\eta = 0$ demonstrates by Eq. (16c) a restoring attractive torque and a divergent repulsive torque. The equilibrium point is locally stable if the commanding spacecraft is repulsive, craft with opposite potential signs, whereas the equilibrium is locally unstable if the torque is attractive, craft with same potential sign.

Case 2: Now assume that the cylinder is pitched to $\Phi = 90^\circ$. Equilibrium in Eq. (16b) requires that either $\dot{\Phi} = 0$ or $\omega_1 = 0$. Simplifying Eq. (16c) at this configuration requires:

$$I_a\omega_1\eta = 0 \rightarrow \begin{cases} \omega_1 \neq 0 & \text{then } \eta = 0 \\ \omega_1 = 0 & \text{then } \eta = \text{const.} \end{cases} \tag{19}$$

The equilibria conditions demonstrate that if any cross coupling from ω_1 is present, then $\dot{\Phi} = 0$ and $\eta = 0$. Otherwise only the projection angle rate is controlled. The stability of this configuration is studied by inserting perturbations in both η and Φ. Unlike the prior case, the torque axis is well defined and therefore perturbations exclusively in η are possible. In the trivial case, where $\omega_1 = 0$, the perturbation in η is not coupled and η increases by the perturbation to assume a new constant value. This characterizes a neutrally stable configuration. The non-trivial case with ω_1 coupling is described by the following linearized equations:

$$I_t\Delta\dot{\eta} - I_a\omega_1\Delta\dot{\Phi} = 0 \tag{20a}$$

$$I_t(\Delta\ddot{\Phi} + \eta^2\Delta\Phi) + I_a\omega_1\Delta\eta = 2f(\phi)\Delta\Phi \tag{20b}$$

Evaluation of Eq. (20) for positive $\Delta\eta$ demonstrates a negative $\ddot{\Phi}$. The body transitions to a state of tumble with exchange between η and $\dot{\Phi}$. The tumble endures torque and angular momentum loss in both attractive and repulsive cases. Given a repulsive electrostatic torque, that is $f(\phi) > 0$, drives the system to the equilibrium condition and is locally stable. The attractive electrostatic torque is destabilizing and drives the tumble away from the equilibrium configuration and is locally unstable. Given the cylinder's symmetric properties, the presented cases fully describe all equilibrium

orientations possible from the observation that a projection angle $\pi/2 < \Phi \leq \pi$ is equivalent to the orientations $\pi - \Phi$.

FEEDBACK CONTROL DEVELOPMENT

The following feedback control development uses rotation rate control to reduce or eliminate the cylinder's tumbling motion. A fixed separation distance is maintained using the inertial thrusting scheme described in Reference 5. The controller assumes the projection angle Φ and angle rate $\dot{\Phi}$ are measured and the commanding spacecraft potential ϕ_1 is the control variable.[5] The feedback control $f(\phi_1)$ is used:

$$f(\phi_1) = -\text{sgn}\left(\sum_{m=1}^{n} g_m(\sigma)\right) h(\alpha\dot{\sigma}) \tag{21}$$

where $\alpha > 0$ is a constant feedback gain and the function h is chosen for stability such that:[5]

$$h(x)x > 0 \quad \text{if } x \neq 0 \tag{22}$$

Tumble rates that tend toward infinity necessitate a limit on physical potential. The following h function proposed by Reference 5 smoothly limits, or saturates, the control at a maximum potential.

$$h(\alpha\dot{\sigma}) = f(\phi_{\text{max}})\frac{\arctan(\alpha\dot{\sigma})}{\pi/2} \tag{23}$$

that is

$$\lim_{\dot{\sigma}\to+\infty} f(\phi_1) = \begin{cases} f(\phi_{\text{max}}) & \text{if } \sum_{m=1}^{n} g_m(\sigma) \neq 0 \\ 0 & \text{if } \sum_{m=1}^{n} g_m(\sigma) = 0 \end{cases} \tag{24}$$

Stability Analysis

The stability of the proposed feedback control law in Eq. (21) is explored using a fundamental positive definite candidate Lyapunov function in Eq. (25). The proposed rate control arrests the rotational motion about the transverse cylinder axis and does not seek to arrest the rotational motion about the axi-symmetric body axis nor achieve a specific spacecraft orientation.

$$V = \frac{1}{2}\boldsymbol{\omega}^T I \boldsymbol{\omega} \tag{25}$$

Taking the time derivative of the candidate Lyapunov function with no torques around the $\hat{\boldsymbol{b}}_1$ axis produces

$$\dot{V} = \boldsymbol{\omega}^T \boldsymbol{L} = \omega_2 L_2 + \omega_3 L_3 \tag{26}$$

Applying the definitions presented in Eq (17), the Lyapunov function derivative assumes the form

$$\dot{V} = -L\left(-\dot{\Phi}\sin\Phi\right) = f(\phi_1)\dot{\Phi}\sin\Phi\sum_{m=1}^{n}\gamma_m\sin(2m\Phi) \tag{27}$$

Substituting in the proposed control law presented of Eq. (21) into the Lyapunov derivative in Eq. (27) yields the final form

$$\dot{V} = -\text{sgn}\left(\sum_{m=1}^{n} g_m(\Phi)\right) h(\alpha\dot{\Phi})\dot{\Phi}\sin\Phi \leq 0 \tag{28}$$

The $\dot{V}$ expression is globally negative semi-definite as the orientation dependence summation is positive semi-definite and the h function is positive definite and $\sin(\Phi)$ is positive semi-definite in the range considered. The symmetry of this treatment enables the projection angle to be bounded by $-\pi/2 < \Phi \leq \pi/2$. The bound is justified by the equivalence between a projection angle of $\pi/2 < \Phi \leq \pi$ and a redefined $\hat{\boldsymbol{b}}_1$ to align with the approaching slender axis with $-\pi/2 < \Phi \leq 0$.

The formulation in Eq. (21) is still a valid control formulation if only positive or negative potential, mono-polarity, is available for the commanding spacecraft. As Reference 5 discusses, the mono-polarity case does not impact the arguments for stability. Implementation of a mono-polarity controller would determine the sign of Eq. (21) to retain only the desired sign and zero-out any opposing sign command.

NUMERICAL SIMULATION

A numerical simulation is performed to verify the control scheme developed. Specifically, a rate-control in deep space with a fixed separation distance is implemented. The fixed separation distance is maintained using inertial thrusting. The MSM model parameters are presented in Table 1 and the simulation parameters are shown in Table 2.

Table 2. Simulation parameters for cylinder detumble system.

Parameter	Value	Units	Description
ρ	100	kg/m^3	Object densities
m_1	52.4	kg	Commanding Sphere mass
m_2	235.6	kg	Cylinder mass
I_a	29.5	kg·m^2	Cylinder axial moment of inertia
I_t	191.4	kg·m^2	Cylinder transverse moment of inertia
ω_0	0.2	deg/sec	Initial cylinder tumble rate
α	5×10^4	-	Gain in h function
ϕ_{max}	20	kV	Max voltage in h function

First consider the cylinder yawed by $\theta = 45^\circ$ and with zero pitch with body frame angular velocities $\boldsymbol{\omega} = [0.0063, 0.1971, 0.0338]$ deg/sec. While the angular velocity of the body is below the MDA maximum of 1°/sec, using a magnitude of 0.2°/sec allows visualization of the long term behavior on a shorter time scale. The numerical simulation using the prescribed initial conditions is shown in Figure 6.

The simulation in Figure 6 converges to the cross-track equilibrium state shown in Figure 6(b). As expected for a fixed separation distance without nominal tugging or pushing, Figure 6(a) shows that the commanded potential goes to the nominal zero value. The equilibrium analysis about this configuration suggested that the value of η remain constant. The bounded angular velocity oscillations in Figure 6(c) indicate that η is constant in a torque free configuration. The convergence to the cross-track equilibrium state shown in Figure 6 lacks electrostatic control authority. Repositioning the commanding spacecraft to the plane of rotation allows complete control authority. This case is explored in Figure 7.

The simulation in Figure 7 converges to $\Phi = 0$. The controller first removes the majority of angular velocity and tends towards the constant magnitude of ω_1. The controller maintains a slightly

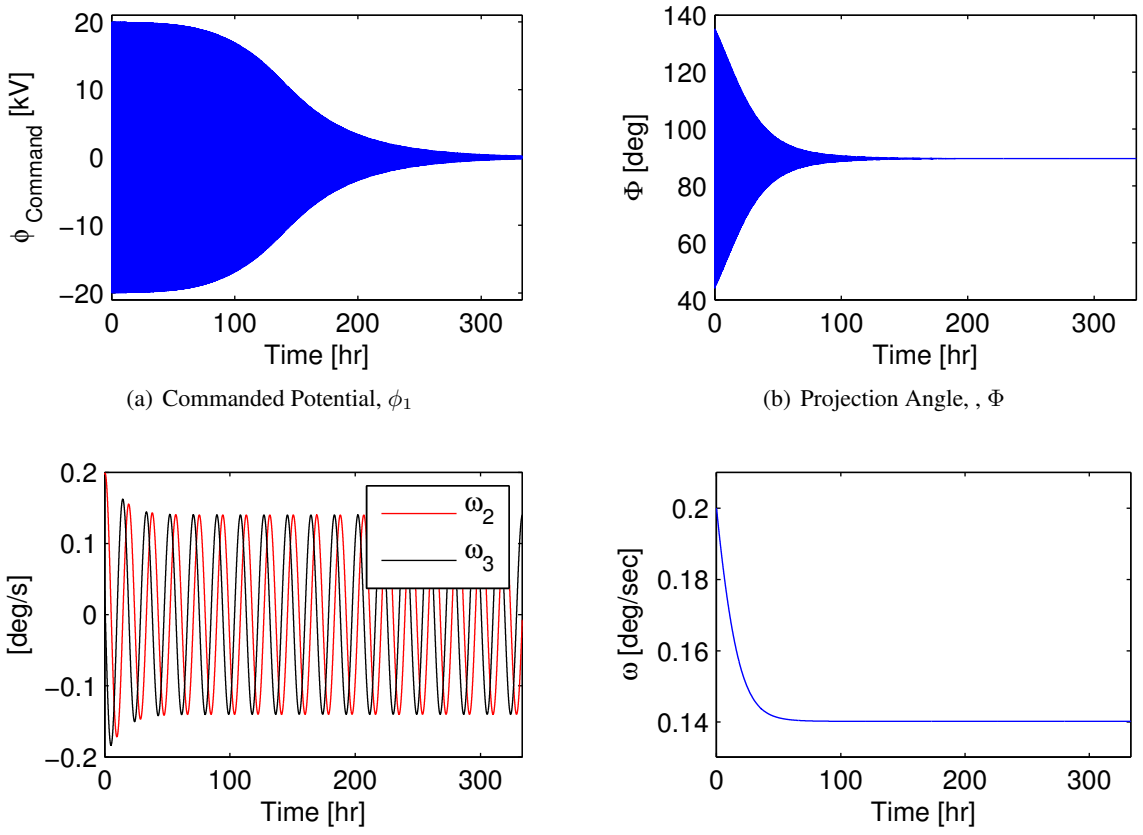

(a) Commanded Potential, ϕ_1

(b) Projection Angle, , Φ

(c) Angular velocity components, $\boldsymbol{\omega}$

(d) Angular velocity magnitude, $|\omega|$

Figure 6. Numerical simulation with initial conditions: $|\omega| = 0.2$**,** $d = 15$ **m,** $\Phi_0 = 45°$**, with** $V_{\max} = 20\ kV$**.**

positive potential due to slight oscillation in the angular velocities that continues to drive the projection angle to the torque free attitude. The decreasing magnitude of the command potential is not discernible in Figure 7(a), however the magnitude goes to zero as the projection angle goes to zero. The initial angular velocity presented is not large in magnitude, however it is large given the small commanding spacecraft dimensions and large separation distance. The presented control formulation seeks to arrest only the projection angle rate. Inclusion of a coast phase or spacecraft reorientation could achieve the desired projection angle after the projection angle rate is zero. The numerical simulations presented in Figure 6 and Figure 7 demonstrate the control implementation for three dimensional electrostatic detumble that can remove angular momentum from large orbital objects within days.

CONCLUSION

The rate-based electrostatic attitude control is investigated for the three-dimensional tumbling motion of a representative cylindrical body. The electrostatic control authority at separation distances on the order of 3-4 craft radii demonstrates that the tumbling rotational motion is greatly reduced. More rapid detumble is possible with reduced separation distance. The control scheme utilizes a general approximation of the multi-sphere modeling method to verify closed-loop stabil-

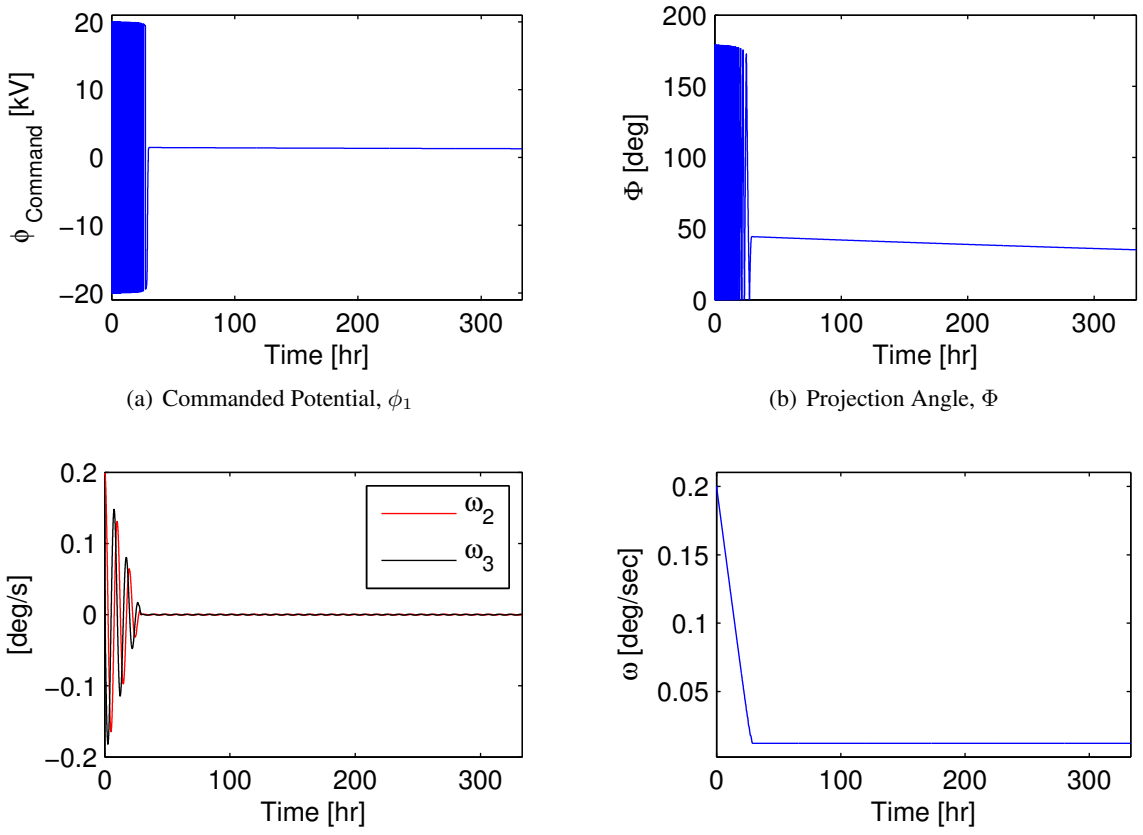

(a) Commanded Potential, ϕ_1

(b) Projection Angle, Φ

(c) Angular velocity components, $\boldsymbol{\omega}$

(d) Angular velocity magnitude, $|\omega|$

Figure 7. Numerical simulation using previous initial conditions with $\Phi_0 = 0°$.

ity. The general approximation generalizes previous work and enables stability analysis for close-proximity distances. The control scheme is analytically proven to arrest the tumbling motion and settle in a stable torque equilibrium orientation. The numerical simulation also highlights the movement towards specific orientations dependent on initial orientation. Future work will analyze the initial orientation dependencies, three-dimensional nominal tugging or pushing, control coast segments, and investigate the torques on more complex geometries.

REFERENCES

[1] P. Couzin, F. Teti, and R. Rembala, "Active Removal of Large Debris: System approach of deorbiting concepts and Technological issues," *6th European Conference on Space Debris*, Darmstadt, Germany, April 22–25 2013. Paper No. 6a.P-17.

[2] A. Ogilvie, J. Allport, M. Hannah, and J. Lymer, "Autonomous satellite servicing using the orbital express demonstration manipulator system," *Proc. of the 9th International Symposium on Artificial Intelligence, Robotics and Automation in Space (i-SAIRAS'08)*, 2008, pp. 25–29.

[3] W. Xu, B. Liang, B. Li, and Y. Xu, "A universal on-orbit servicing system used in the geostationary orbit," *Advances in Space Research*, Vol. 48, No. 1, 2011, pp. 95–119, 10.1016/j.asr.2011.02.012.

[4] P. Couzin, F. Teti, and R. Rembala, "Active Removal of Large Debris : Rendez-vous and Robotic Capture Issues," *2nd European Workshop on Active Debris Removal*, Paris, France, 2012. Paper #7.5.

[5] H. Schaub and D. Stevenson, "Prospects Of Relative Attitude Control Using Coulomb Actuation," *Jer-Nan Juang Astrodynamics Symposium*, College Station, TX, June 25–26 2012. Paper AAS 12–607.

[6] H. Schaub and D. F. Moorer, "Geosynchronous Large Debris Reorbiter: Challenges and Prospects," *AAS Kyle T. Alfriend Astrodynamics Symposium*, Monterey, CA, May 17–19 2010. Paper No. AAS 10-311.

[7] D. F. Moorer and H. Schaub, "Hybrid Electrostatic Space Tug," US Patent 0036951-A1, Feb. 17 2011.

[8] D. F. Moorer and H. Schaub, "Electrostatic Spacecraft Reorbiter," US Patent 8,205,838 B2, Feb. 17 2011.

[9] N. Murdoch, D. Izzo, C. Bombardelli, I. Carnelli, A. Hilgers, and D. Rodgers, "Electrostatic tractor for near Earth object deflection," *59th International Astronautical Congress*, Glasgow Scotland, 2008. Paper IAC-08-A3.I.5.

[10] N. Murdoch, D. Izzo, C. Bombardelli, I. Carnelli, A. Hilgers, and D. Rodgers, "The Electrostatic Tractor for Asteroid Deflection," *58th International Astronautical Congress*, 2008. Paper IAC-08-A3.I.5.

[11] J. H. Cover, W. Knauer, and H. A. Maurer, "Lightweight Reflecting Structures Utilizing Electrostatic Inflation," US Patent 3,546,706, October 1966.

[12] L. B. King, G. G. Parker, S. Deshmukh, and J.-H. Chong, "Spacecraft Formation-Flying using Inter-Vehicle Coulomb Forces," tech. rep., NASA/NIAC, January 2002. `http://www.niac.usra.edu`.

[13] J. Berryman and H. Schaub, "Analytical Charge Analysis for 2- and 3-Craft Coulomb Formations," *AIAA Journal of Guidance, Control, and Dynamics*, Vol. 30, Nov.–Dec. 2007, pp. 1701–1710.

[14] C. R. Seubert, S. Panosian, and H. Schaub, "Analysis of a Tethered Coulomb Structure Applied to Close Proximity Situational Awareness," *AIAA Journal of Spacecraft and Rockets*, Vol. 49, Nov. – Dec. 2012, pp. 1183–1193.

[15] L. A. Stiles, H. Schaub, K. K. Maute, and D. F. Moorer, "Electrostatically inflated gossamer space structure voltage requirements due to orbital perturbations," *Acta Astronautica*, Vol. 84, Mar.–Apr. 2013, pp. 109–121, 10.1016/j.actaastro.2012.11.007.

[16] S. Wang and H. Schaub, "Nonlinear Charge Control for a Collinear Fixed Shape Three-Craft Equilibrium," *AIAA Journal of Guidance, Control, and Dynamics*, Vol. 34, Mar.–Apr. 2011, pp. 359–366, 10.2514/1.52117.

[17] M. A. Peck, "Prospects and Challenges for Lorentz-Augmented Orbits," *AIAA Guidance, Navigation and Control Conference*, San Francisco, CA, August 15–18 2005. Paper No. AIAA 2005-5995.

[18] B. Streetman and M. A. Peck, "New Synchronous Orbits Using the Geomagentic Lorentz Force," *AIAA Journal of Guidance, Control, and Dynamics*, Vol. 30, Nov.–Dec. 2007, pp. 1677–1690.

[19] D. Stevenson and H. Schaub, "Multi-Sphere Method for Modeling Electrostatic Forces and Torques," *Advances in Space Research*, Vol. 51, Jan. 2013, pp. 10–20, 10.1016/j.asr.2012.08.014.

[20] D. Stevenson, "Optimization of Sphere Population for Electrostatic Multi Sphere Model," *12th Spacecraft Charging Technology Conference*, Kitakyushu, Japan, May 14–18 2012.

[21] D. Stevenson and H. Schaub, "Rotational Testbed for Coulomb Induced Spacecraft Attitude Control," *5th International Conference on Spacecraft Formation Flying Missions and Technologies*, Münich, Germany, May 29–31 2013.

[22] W. R. Smythe, *Static and Dynamic Electricity*. McGraw–Hill, 3rd ed., 1968.

[23] J. Sliško and R. A. Brito-Orta, "On approximate formulas for the electrostatic force between two conducting spheres," *American Journal of Physics*, Vol. 66, No. 4, 1998, pp. 352–355.